Pure Appl. Chem., Vol. 78, No. 6, pp. 1187–1202, 2006.
doi:10.1351/pac200678061187

Radical-surface interactions during film deposition: A sticky situation?*

Dongping Liu, Ina T. Martin, Jie Zhou, and Ellen R. Fisher‡

Department of Chemistry, Colorado State University, Fort Collins, CO 80523-1872, USA

Abstract: Our imaging of radicals interacting with surfaces (IRIS) method was used to investigate radical-surface reactions during low-temperature plasma-enhanced chemical vapor deposition (PECVD) processes. Special emphasis was placed on the analysis of surface reactivities for CH, SiH, CN, NH, NH_2, CF_2, and $SiCl_2$ radicals during film growth. The effects of plasma parameters, such as radio frequency (rf) power and gas composition, substrate temperature, and substrate bias on radical-surface reactivity were analyzed. Different radicals exhibit different behavior at the surface of a depositing film. Specifically, CH, SiH, and CN are "sticky", with high surface reactivities. In contrast, other species such as NH, CF_2, and $SiCl_2$ do not stick to the surface of growing films and, in some cases are actually generated at the surface of the depositing film. Different plasma systems and parameters can have an effect on the stickiness of some of these species. Our IRIS measurements indicate a molecule's surface sticking probability may also be related to the molecule's electronic configuration and stability, with the most reactive species being molecules with a doublet electron configuration. In contrast, the singlet species examined here tend to be generated at the surface during film deposition. Our results also indicate that when a molecule scatters with greater than 100 % probability, it is likely to be strongly affected by energetic ion bombardment of the film surface.

Keywords: PECVD; LIF; radicals; surface reactivity.

INTRODUCTION

Amorphous carbon- and silicon-based materials are widely used for an ever-increasing number of applications. Often, these materials can be deposited via plasma-enhanced chemical vapor deposition (PECVD), resulting in films with unique physical and chemical properties. A variety of carbon- and silicon-based plasmas have been used to tailor the resulting materials properties. These include: (1) diamond-like carbon (DLC) or amorphous, hydrogenated carbon (a-C:H) films prepared from hydrocarbon precursors such as methane and ethane. DLC materials are widely used as protective coatings owing to their extraordinary material properties such as extreme hardness, low friction coefficients, chemical inertness, and infrared transparency [1,2]. (2) Amorphous carbon nitride (a-C:N) films, deposited from hydrocarbon/N_2 (or NH_3) plasmas, have been proposed as an ideal material for wear-resistant hard coatings, protective optical coatings, and also as a novel semiconductor material [3,4]. (3) Amorphous fluorocarbon (a-FC) films from a variety of perfluoro- and fluorinated, hydrogenated compounds are attractive materials with numerous applications based on film properties such as low di-

*Paper presented at the 17th International Symposium on Plasma Chemistry (ISPC 17), Toronto, Ontario, Canada, 7–12 August 2005. Other presentations are published in this issue, pp. 1093–1298.

‡Corresponding author

electric constants, high hydrophobicity, low friction coefficients, chemical inertness, and biocompatibility [5–7]. (4) Hydrogenated amorphous silicon (a-Si:H) films deposited from plasmas comprising SiH_4, Si_2H_6, or H_2-diluted chlorinated silanes such as SiH_2Cl_2 and $SiCl_4$ have their primary applications in solar cells, thin film transistors, and detectors [8–10].

In all these systems, film formation and properties are determined by the interactions of various plasma species with the surface of the growing film, yet relatively little is known about the molecular-level processes that occur in the gas phase and at the plasma–surface interface. In particular, transient species created in the plasma are thought to be key actors in the deposition of a wide variety of film types. For the remainder of this article, we will follow Herzberg's [11] example and use the term "radical" to refer to coordinately unsaturated species created by the decomposition of coordinately saturated molecules, rather than limiting the term to those species with an unpaired electron. Indeed, radical-surface reactions are believed to be the key steps leading to deposition of amorphous films in DLC, a-FC and Si-based PECVD systems.

In general, it is assumed that when radicals impinge on a surface, they react with unit probability. Indeed, this assumption is regularly made in computer simulations of plasma processes where no experimental data is available [12,13]. This "sticking" or surface loss can occur via several different processes, including abstraction of a bonded surface atom or recombination with another radical, molecule, or dangling bond at the surface. For example, von Kuedell and coworkers have investigated the simultaneous interaction of CH_3 and H radicals with a-C:H films using optical in situ diagnostics [14,15]. They found that the sticking coefficient of CH_3 radicals is related to the surface radical site or "dangling bond" density. These sites are created by H radicals through abstraction of surface hydrogen atoms; impinging CH_3 radicals then adsorb at these dangling bonds, leading to the growth of a-C:H films. Likewise, in silicon deposition systems, among the primary dissociation products of SiH_4, the SiH_3 radical is widely accepted as the main precursor of the a-Si:H films, although SiH_n radicals (n = 0–2) are believed to have a significant effect on the film quality [16–19]. In FC plasmas, CF_x (x = 1–3) radicals have been proposed as critical components in the polymerization process forming a-FC films [6,20–22]. These radicals are thought to contribute to polymer growth by reacting with "activated" sites in the polymeric surface, or by forming addition compounds through gas-phase reactions with other radicals or unsaturated species. Despite these predicted behaviors, the basic growth mechanisms for the PECVD method still remain unclear. Thus, to understand film growth mechanisms, it is critical to monitor the surface reactivity of radicals *during* plasma-surface interactions.

Currently, only a limited number of techniques are available to determine the surface reaction probability of plasma radicals, including time-resolved measurements of radical densities in pulsed plasmas [23,24] and the measurements of spatial concentration profiles near reactor walls [25,26]. The extraction of the surface reaction probability from these data generally requires extensive modeling of the diffusional transport equations for the plasma. One method that requires fewer calculations is our imaging of radicals interacting with surfaces (IRIS) technique. With IRIS, the surface reactivity of radicals during plasma-surface interactions is directly measured by two-dimensional imaging using laser-induced fluorescence (LIF). Thus, IRIS enables the exploration of the dependence of the surface reactivity on various plasma parameters (gas composition, pressure, applied rf power), substrate temperature, material, and bias, as well as ion bombardment. In addition, IRIS measurements also allow characterization of gas-phase plasma species generated at the substrate surface during film deposition.

IRIS has previously been used to explore the surface interactions of small molecules in numerous plasma deposition systems [27,28]. Here, we present a broad array of IRIS data to demonstrate the capabilities of the IRIS technique and to explore the validity of some common hypotheses made regarding radical–surface interactions. Specifically, we present data for CH in CH_4 and CH_4/Ar plasmas used for a-C:H deposition; CN, NH, and NH_2 in CH_4/N_2 and CH_4/NH_3 plasmas used for a-C:N:H deposition; SiH in SiH_4, SiH_4/N_2, and SiH_4/CH_4 plasmas during deposition of amorphous silicon-based materials; CF_2 in C_3F_8 and C_4F_8 plasmas during deposition of a-FC; and $SiCl_2$ in $SiCl_4/H_2$ plasmas used for a-Si:H deposition. In these systems, the surface reactivity of radicals is determined, and the effects

of various experimental parameters on the surface reactivity are analyzed. These data will allow us to examine the following common hypotheses: (1) All radicals have unit sticking probability on any surface under all conditions; and (2) a radical's surface reactivity is an inherent property of the radical. The first of these is based largely on the observation that radicals are reactive species with high reaction probabilities, whereas the second can be associated with the electronic structure of the molecule. For example, in gas-phase reactivity data, with the isoelectronic $O(^3P)/O(^1D)$, NH, and CH_2 triplet/singlet pairs, the singlet species are found to be highly reactive and to undergo bond insertion more readily than the triplet species [29,30]. Thus, a third hypothesis is that isoelectronic species would have similar surface reactivities. Finally, it is also useful to consider how the surface reactivity of one plasma species is affected by the presence of other plasma species.

EXPERIMENTAL DETAILS

IRIS is used to measure the steady-state surface reactivity of radicals during plasma processing of a substrate, as well as the relative gas-phase density of plasma species as a function of different plasma parameters (applied rf power (P), pressure, and gas composition), substrate temperature (T_S), and substrate bias. The IRIS apparatus has been described in detail previously [31]. Briefly, in a typical IRIS experiment, feed gases enter a cylindrical, glass tubular reactor. A nickel-plated copper coil is used to couple 13.56 MHz rf power (10–200 W) to the glass reactor, and a plasma is produced. Expansion of the plasma through a differentially pumped high vacuum system generates an effusive molecular beam, which contains virtually all the species present in the plasma. The molecular beam is collimated by two slits mounted on a liquid nitrogen-cooled shield, which can be maintained at –160 °C during data collection. This serves to minimize spurious scattering off the differential wall for radical reactivity measurements.

A tunable excimer-pumped (XeCl) dye laser beam intersects the molecular beam at a 45° angle downstream from the plasma source and excites the selected molecule. Spatially resolved LIF signals are collected by a gated, intensified charge-coupled device (ICCD) located perpendicular to both the molecular beam and the laser beam, directly above the interaction region. For fluorescence excitation spectra, tunable laser light is produced from an excimer pumped dye laser. Total fluorescence produced by a particular radical transition is collected and plotted as a function of laser wavelength. For density measurements, LIF intensity produced by a particular transition is collected as a function of plasma parameters such as the feed gas composition or P. For reactivity measurements, a Si substrate mounted on a copper substrate holder is rotated into the path of the molecular beam, and LIF signals are again collected. Differences between the spatial distributions with the substrate surface in and out of the path of the molecular beam are used to measure the amount of scattering (alternatively, surface reactivity), for a particular radical. In general, LIF signals were acquired with multiple accumulations of 500–10 000 counts/accumulation and multiple sets of data collected for each experiment. Background images, acquired with the laser tuned to an off-resonance wavelength, were subtracted from the corresponding on-resonance image. For measurements in chlorosilane plasmas, background images were collected with the laser off.

For reactivity measurements, one-dimensional cross-sections of beam and scatter images were made by averaging a column 20 pixels wide (an 8.0 mm swath) containing the LIF signal and plotting signal intensity as a function of distance along the laser-beam path. These spatially resolved LIF data were interpreted using a quantitative model of the experiment that reproduces the scattering data in one dimension. A complete description of the model is given elsewhere [32]. It is based on the known experimental geometry and calculates the spatial distribution of the radical number density in the molecular beam at the interaction region as well as those for the radicals scattering from the substrate surface. To adequately describe the spatial distribution of molecules from the substrate, an adsorption–desorption scattering mechanism is assumed. The calculated curve for this type of scatter assumes that all incident radicals leave the surface with a cosine distribution about the surface normal. The scattering co-

efficient, *S*, defined as the ratio of the flux of scattered molecules to that of molecules in the incident beam, is adjusted to best fit the experimental data. The surface reactivity, *R*, is defined as 1-*S*. For molecules that are produced at the surface, IRIS results are generally presented in terms of *S*, whereas molecules that are lost at the surface are presented in terms of *R*. Ion effects were studied by applying +200 V bias on the substrate to repel positively charged species or by placing a grounded mesh (g.m.) into the path of the molecular beam to remove the charged species.

The surface reactivities of various plasma species were measured at the surface of a growing film in different deposition systems. Relevant IRIS conditions for the reactivity measurements of these species are listed in Table 1, along with their radiative lifetimes [33–39]. In general, for each species, fluorescence was collected over the entire radiative lifetime of the radical's transition states. Tunable laser light for the excitation of a particular radical was produced using different laser dyes, Table 1. The plasma molecular beam was collimated by two slits, 1.0–1.6 and 0.8–1.7 mm wide, respectively, with the second slit located 12 mm downstream from the first slit. For NH_x, CF_2, and $SiCl_2$ measurements, the two slits were cooled by liquid nitrogen and maintained at –160 °C during data collection. In general, the ICCD camera had a 1.0 μs gate width, and a 1.65 μs gate delay. The distance between the laser beam and the substrate surface was kept between 3.0 and 3.6 mm for reactivity experiments.

Table 1 IRIS conditions for radical reactivity measurements.

Radical	Transition	Radiative lifetime	Wavelength (nm)		Laser dye	Slit sizes (mm)		Liquid nitrogen cooling	ICCD camera	
			On-resonance	Off-resonance		First	Second		Gate width	Gate delay
CH	$A^2\Delta \rightarrow X^2\Pi$	537 ns [33]	430.402	430.200	Coumarin 440	1.6	1.7	–	2.0 μs	1.68 μs
CN	$B^2\Sigma^+ \rightarrow X^2\Sigma^+$	61 ns [37]	387.145	387.500	Excile 0389	1.6	1.7	–	1.0 μs	1.68 μs
NH	$A^3\Pi \rightarrow X^3\Sigma^-$	440 ns [34]	336.072	336.050	*p*-Terphenyl	1.5	1.6	–160 °C	1.0 μs	1.65 μs
NH_2[a]	$^2A_1 \rightarrow {}^2B_1$	10 μs [36]	597.730	597.900	Rhodamine 6G	2.0	2.0	–160 °C	1.0 μs	1.65 μs
SiH	$A^2\Delta \rightarrow X^2\Pi$	534 ns [62]	413.418	413.440	Excalite 417	1.0	0.8–1.2	–	2.0 μs	1.65 μs
CF_2	$A^1B_1 \rightarrow X^1A_1$	61 ns [38]	234.323	235.000	Coumarin 47	1.0–1.1	1.2–1.4	–160 °C	100 ns	1.65 μs
$SiCl_2$	$A^1B_1 \rightarrow X^1A_1$	4.5 μs [39]	320.340	Laser off	Sulforhodamine	1.6	1.7	–160 °C	1.0 μs	1.65 μs

[a]The transition studied here is primarily from three overlapping rotational bands of the Σ(0,9,0) vibronic state.

Mass spectrometry measurements were conducted using a Hiden PSM003 quadrupole mass spectrometer (MS). The MS was mounted onto the IRIS main chamber directly in line with the plasma molecular beam, at approximately the position of the interaction region. This results in the analysis of the ions that bombard the substrate surface during reactivity measurements. Details of the experimental setup are given elsewhere [40–42]. For data presented here, the ionizer on the MS was disabled to permit identification and detection of the nascent ions in the plasma. The MS identifies various ions according to their mass-to-charge (m/q) ratio, and the ion energy distribution (IED) is measured individually for each m/q selected ion as a function of *P* (25–150 W). The density of negative ions in our plasmas is extremely low [43]; thus, the signal of negative ions is below the detection limit of the MS. The data presented here are the first IEDs measured directly on the IRIS chamber.

RESULTS

Spectroscopy

LIF is a nonintrusive and highly selective technique that allows for the identification and study of one type of species among many others in the plasma molecular beam. In principal, the tunable XeCl dye laser beam (200–800 nm) can excite various radicals during film deposition for IRIS measurements.

Figure 1 contains the fluorescence excitation spectra collected from CH_4/NH_3, CH_4/N_2, and CH_4 plasmas over three different wavelength ranges. Comparison to the literature verifies the presence of NH ($A^3\Pi \rightarrow X^3\Sigma^-$), CN ($B^2\Sigma^+ \rightarrow X^2\Sigma^+$), and CH ($A^2\Delta \rightarrow X^2\Pi$), in the 335–338, 386–388, and the 430–431 nm ranges, respectively. For each species, there is no interference from other fluorescing species in the wavelength ranges studied. Thus, we can examine the reactivity of all three of these molecules as well as NH_2 (data not shown) in the same plasma systems (e.g., the CH_4/N_2 and CH_4/NH_3 plasmas used to deposit a-C:N films) under the same conditions.

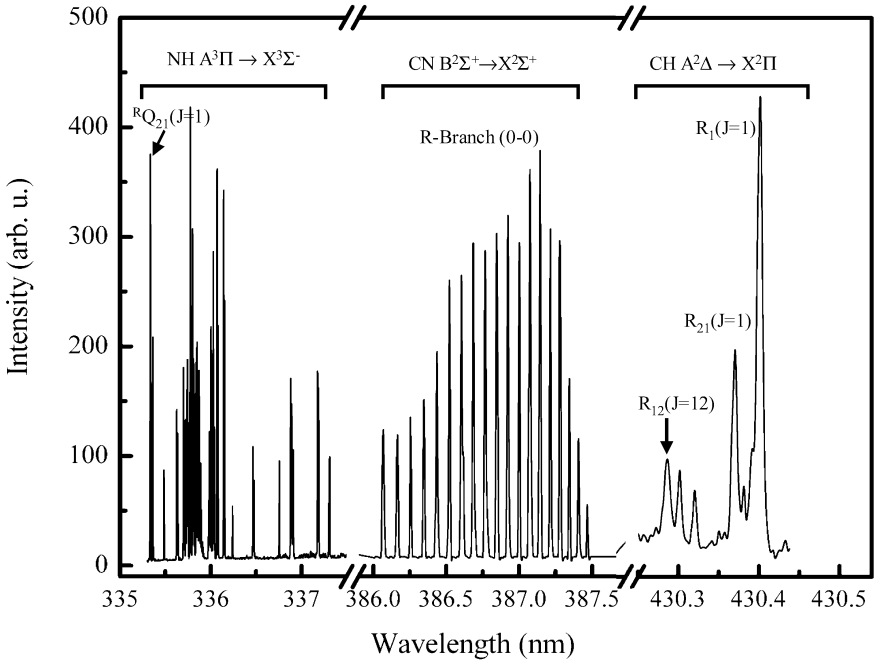

Fig. 1 Experimental fluorescence excitation spectra of the NH $A^2\Pi \rightarrow X^3\Sigma^-$ (0, 0) transition in a CH_4/NH_3 plasma (P = 100 W); the CN $B^2\Sigma^+ \rightarrow X^2\Sigma^+$ (0, 0) transition in a CH_4/N_2 plasma (P = 110 W); and the CH $A^2\Delta \rightarrow X^2\Pi$ transition in a 100 % CH_4 plasma (P = 100 W).

Excitation spectra are used not only to identify molecules created in the plasma, but comparison of relative line intensities between experimental and calculated spectra allow the measurement of the rotational temperature (Θ_R) of diatomic plasma species. For the data presented in Fig. 1, Θ_R(NH) = 390 ± 40 K at P = 100–110 W, Θ_R(CN) = 400 ± 50 K at P = 110 W, and Θ_R (CH) = 1450 ± 50 K at P = 50–150 W. The first two of these are similar to values measured for other radicals in our plasma systems such as SiH (Θ_R = 600 ± 40 K at P = 20–80 W [44]) and OH (Θ_R = 450 ± 20 K at P = 85 W [32]). However, Θ_R(CH) is considerably hotter than all of these other values. This level of increased rotational temperature for CH has been observed previously in CH_4-based plasmas [45,46].

Figure 2a shows the LIF signal intensities of NH_2 in CH_4/N_2 plasmas, CH in CH_4/Ar plasmas, and CF_2 in C_4F_8 plasmas as a function of applied rf power. The signal intensities show a clear dependence on P, with higher intensities at higher rf powers. In general, increasing P contributes to increased radical generation as a result of increased monomer fragmentation. The intensities of some radicals, however, either level out or decrease at very high P, primarily because of rapid film deposition inside of the reactor. This can be seen in Fig. 2a for CH in the CH_4 system. Similar results have been observed for SiH in SiH_4 plasmas [44]. Gas composition can also affect the densities of plasma species. Figure 2b

shows the CN, NH_2, and NH LIF intensities as a function of NH_3 fraction in 100 W CH_4/NH_3 plasmas. The density of NH and NH_2 increase monotonically when the NH_3 fraction is varied from 10 to 100 %. These results show, as expected, that NH and NH_2 production are directly related to the NH_3 concentration in the plasma. In contrast, CN LIF intensities increase initially with NH_3 fraction, then decrease when the NH_3 fraction exceeds ~40 %. CN in these systems must be formed through gas-phase collisions of carbon and nitrogen containing species, not through simple fragmentation of a monomer gas. Thus the gas-phase density depends on the concentrations of both NH_3 and CH_4.

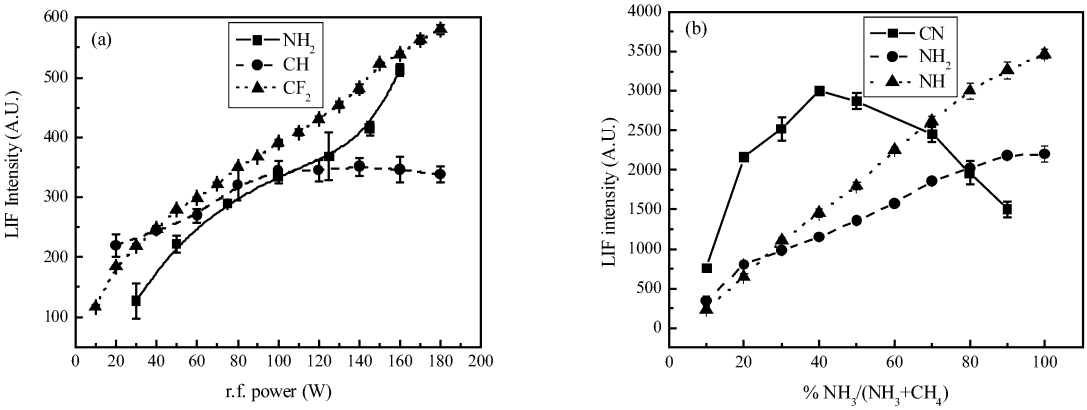

Fig. 2 (a) LIF intensities as a function of applied rf power for NH_2 in 60:40 N_2/CH_4 plasmas (squares), CH in CH_4 plasmas (circles), and CF_2 in C_4F_8 plasmas (triangles); (b) LIF intensities of CN (squares), NH_2 (circles), and NH (triangles) in CH_4/NH_3 plasmas at P = 100 W as a function of the NH_3 fraction in the feed gas.

Radical-surface interactions

Surface reactivity in IRIS experiments is measured by comparison of ICCD images obtained with the substrate in and out of the path of the plasma molecular beam. Figure 3 shows a typical set of 2D ICCD images of LIF signals for CH in a 150 W CH_4 plasma. LIF signal from CH in the incident molecular beam is shown in Fig. 3a. In Fig. 3b, the substrate is placed in the path of the molecular beam and the LIF signal includes both CH in the incident molecular beam and any CH scattered from the substrate surface. The image shown in Fig. 3c is the difference between panels 3b and 3a, showing only a slight signal resulting from CH desorbing from the surface. Figure 4 shows similar IRIS images for $SiCl_2$ from a 100 W, 50:50 $SiCl_4/H_2$ plasma molecular beam interacting with a Si substrate. The difference between the images shown in Figs. 4a and 4b provides a spatially resolved image of $SiCl_2$ radicals scattered from the silicon substrate surface (Fig. 4c). Clearly, in contrast to the CH results, a strong signal resulting from $SiCl_2$ desorbing from the substrate can be seen in this image.

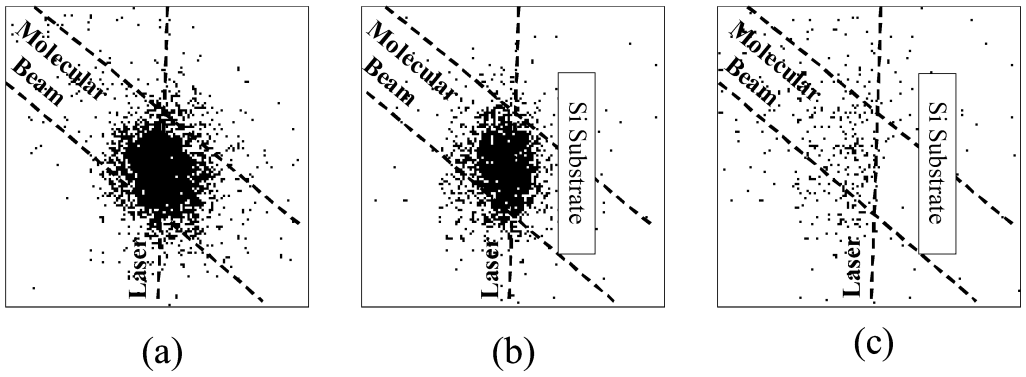

Fig. 3 2D ICCD images of CH LIF signals in (a) a 140 W CH_4 plasma molecular beam and (b) with a 300 K Si substrate rotated into the path of the molecular beam. The image shown in (c) is the difference between the images in (a) and (b) and corresponds to CH radicals scattered from the surface. The metal substrate holder was grounded, and the total gas pressure in the plasma source was 50 mTorr. Dashed lines indicate the locations of the molecular beam and the laser beam.

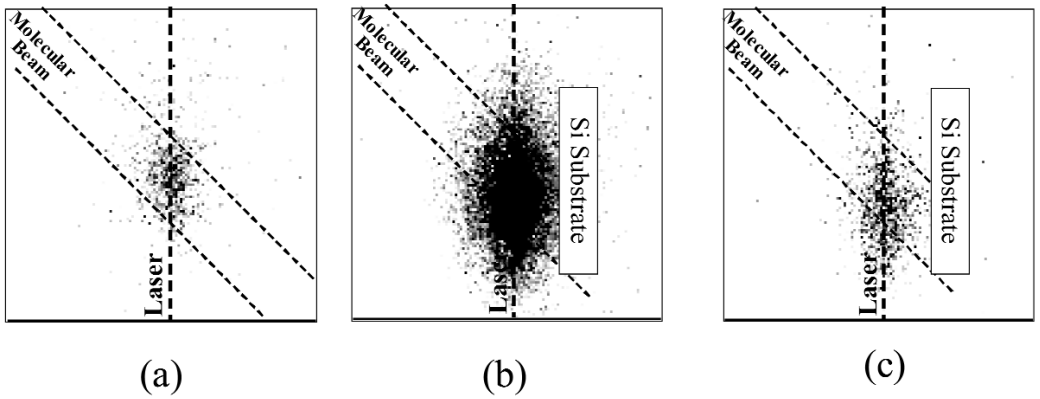

Fig. 4 2D ICCD images of $SiCl_2$ LIF signals in (a) a 50:50 $SiCl_4/H_2$ (P = 100 W) plasma molecular beam and (b) with a 300 K Si substrate rotated into the path of the molecular beam. The image shown in (c) is the difference between the images in (a) and (b) and corresponds to $SiCl_2$ radicals scattered from the surface. The metal substrate holder was grounded, and the total gas pressure in the plasma source was 100 mTorr. Dashed lines indicate the locations of the molecular beam and the laser beam.

To quantify the amount of scatter for a set of reactivity data, 20 columns of pixels were averaged and plotted as a function of distance along the laser axis, Fig. 5. Figure 5a contains the cross-sections of the LIF images of CH shown in Figs. 3a and 3c. The dashed lines are the simulated curves for the incident beam and scattered molecules, assuming an adsorption–desorption mechanism, with $S = 0.01 \pm 0.04$. Figures 5b–5f show representative sets of experimental cross-sections and simulated curves for CN radicals from a 100 W, 60:40 CH_4/N_2 plasma; NH_2 radicals from a 150 W 60:40 CH_4/NH_3 plasma; NH radicals from a 150 W 60:40 CH_4/NH_3 plasma; CF_2 radicals from a 100 W C_3F_8 plasma; and $SiCl_2$ radicals from a 100 W, 50:50 $SiCl_4/H_2$ plasma, respectively. In all systems, these IRIS measurements were made at the surface of films depositing on nonbiased, room-temperature Si substrates. The shift and broadening of the scattered signal from the beam signal that occurs in all these data are consistent with the adsorption–desorption mechanism used in the scatter simulation.

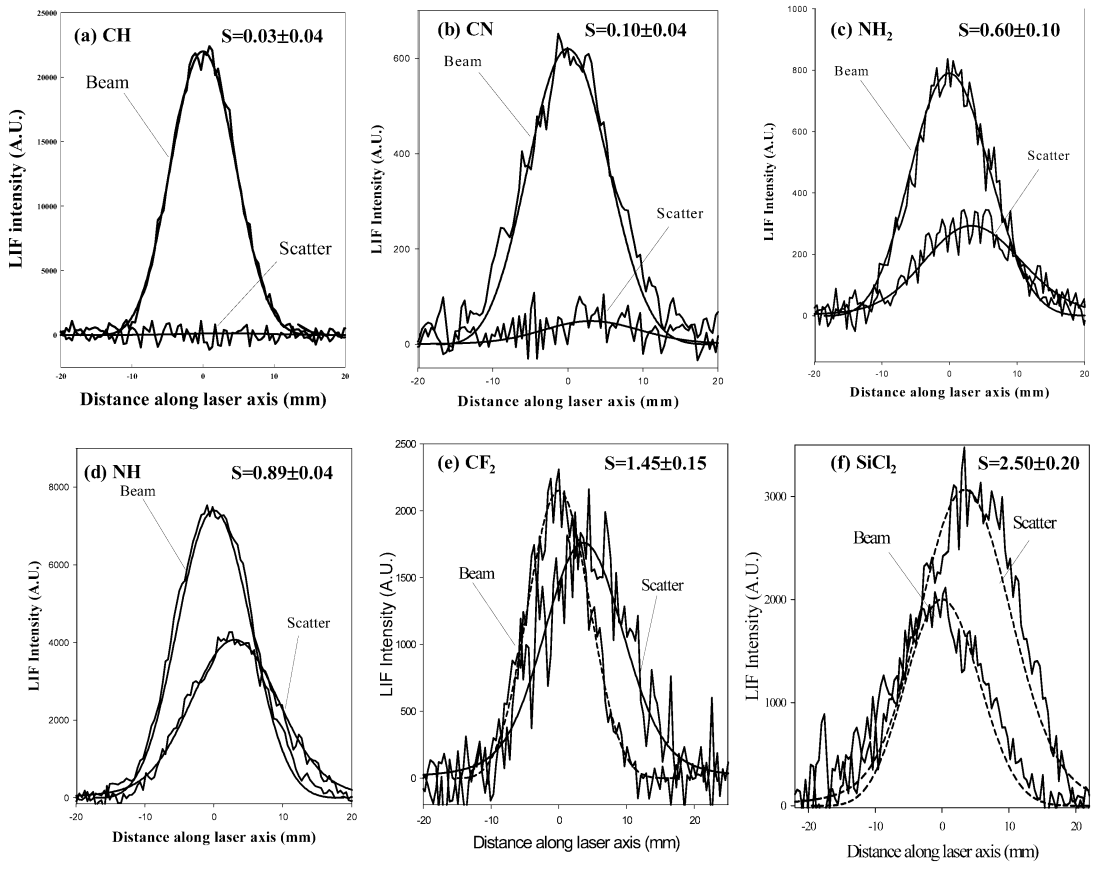

Fig. 5 Representative sets of experimental data and simulated curves for the LIF of (a) CH radicals produced in a 100 % CH_4 (P = 140 W) plasma; (b) CN radicals produced in a 60:40 CH_4/N_2 plasma (P = 100 W); (c) NH_2 radicals produced in a 60:40 CH_4/NH_3 plasma (P = 150 W); (d) NH radicals produced in a 60:40 CH_4/NH_3 plasma (P = 150 W); (e) CF_2 radicals produced in a C_3F_8 plasma (P = 100 W) with no substrate bias; and (f) $SiCl_2$ radicals produced in a 50:50 $SiCl_4/H_2$ plasma (P = 100 W). In all systems, the plasma molecular beams were impinging on unbiased room-temperature Si substrates and amorphous films were being deposited on the substrates.

From Fig. 5, it is apparent that the different radicals studied have very different net scatter behaviors during film growth. The averages of several data sets for the conditions shown in Fig. 5 yield $S(CH) = 0.01 \pm 0.03$, $S(CN) = 0.10 \pm 0.04$, $S(NH_2) = 0.60 \pm 0.10$, $S(NH) = 0.89 \pm 0.04$, $S(CF_2) = 1.45 \pm 0.15$, and $S(SiCl_2) = 2.43 \pm 0.12$. The extremely low S values of CH and CN radicals correspond to high reactivity values [$R(CH) = 0.99 \pm 0.03$ and $R(CN) = 0.90 \pm 0.04$], indicating they are reactive during film growth. In contrast, the $S > 1$ values measured for CF_2 and $SiCl_2$ radicals indicates that net surface generation of these species occurs during film growth. The $0 < S < 1$ values of NH and NH_2 radicals are indicative of moderate surface reactivity.

The effects of gas composition, energetic ions, P, and T_S on the surface reactivity of CH, SiH, CN, NH_2, NH, CF_2, and $SiCl_2$ radicals have been measured, and representative sets of S values are listed in Table 2. Additional data on all of these systems can be found elsewhere [40,42,44,47]. The scattering coefficients of SiH and CH do not show any dependence on feed gas composition or substrate temperature. Indeed, S values for these two molecules are all less than about 0.05 ± 0.07, indicating that nearly 100 % of SiH and CH is lost during the deposition of a-Si:H, a-SiNx:H, a-SiCx:H, and a-C:H films.

Table 2 Surface scattering (S) values for various radicals in film-depositing plasmas.[a]

Radical	System [reference]	Pressure (mTorr)[b]	P (W)	Bias (V)	T_S (K)	Film deposited[b]	S
CH	CH_4 [42]	50	100	0	300–573	a-C:H	0.01 (0.05)
CH	CH_4/Ar [42]	45/5	100	0	300	a-C:H	0.00 (0.05)
CH	CH_4/Ar [42]	40/10	100	0	300	a-C:H	0.01 (0.04)
CH	CH_4/Ar [42]	35/15	100	0	300	a-C:H	0.04 (0.07)
CH	CH_4/Ar [42]	30/20	100	0	300	a-C:H	0.01 (0.05)
SiH	SiH_4 [44]	50	60	0	300	a-Si:H	0.05 (0.05)
SiH	SiH_4/H_2 [44]	10/40	60	0	300	a-Si:H	0.05 (0.07)
SiH	SiH_4/NH_3 [44]	20/30	60	0	300	a-SiNx:H	0.02 (0.05)
SiH	SiH_4/N_2 [44]	35/15	60	0	300	a-SiNx:H	0.03 (0.03)
SiH	SiH_4/CH_4 [44]	25/25	60	0	300	a-SiCx:H	0.04 (0.07)
CN	N_2/CH_4 [47]	30/70	100	+200	300	a-C:N	0.02 (0.10)
CN	N_2/CH_4 [47]	30/70	100	0	300	a-C:N	0.15 (0.10)
NH	NH_3/CH_4 [47]	40/60	150	+200	300	a-C:N	0.87 (0.04)
NH	NH_3/CH_4 [47]	80/20	150	+200	300	a-C:N	0.82 (0.03)
NH	NH_3/CH_4 [47]	40/60	150	0	300	a-C:N	0.87 (0.04)
NH	NH_3/CH_4 [47]	80/20	150	0	300	a-C:N	0.89 (0.02)
NH_2	NH_3/CH_4 [47]	30/70	150	0	300	a-C:N	0.40 (0.10)
NH_2	NH_3/CH_4 [47]	40/60	150	0	300	a-C:N	0.55 (0.10)
NH_2	NH_3/CH_4 [47]	50/50	150	0	300	a-C:N	0.63 (0.05)
NH_2	NH_3/CH_4 [47]	75/25	150	0	300	a-C:N	0.70 (0.10)
NH_2	NH_3/CH_4 [47]	100/0	150	0	300	–	0.80 (0.08)
CF_2	C_3F_8 [40]	45	100	0	300	a-FC	1.56 (0.25)
CF_2	C_4F_8 [40]	45	25	0	300	a-FC	1.27 (0.12)
CF_2	C_4F_8 [40]	45	100	0	300	a-FC	1.61 (0.34)
CF_2	C_4F_8 [40]	45	150	0	300	a-FC	1.65 (0.15)
CF_2	C_4F_8 [40]	45	25	g.m.	300	a-FC	0.90 (0.12)
CF_2	C_4F_8 [40]	45	100	g.m.	300	a-FC	1.07 (0.07)
CF_2	C_4F_8 [40]	45	150	g.m.	300	a-FC	1.30 (0.36)
$SiCl_2$	$SiCl_4$	50	25	0	300	Etching	2.31 (0.04)
$SiCl_2$	$SiCl_4$	50	50	0	300	Etching	3.51 (0.08)
$SiCl_2$	$SiCl_4$	50	80	0	300	Etching	3.90 (0.07)
$SiCl_2$	$SiCl_4$	50	120	0	300	Etching	4.21 (0.07)
$SiCl_2$	$SiCl_4$	50	160	0	300	Etching	4.94 (0.10)
$SiCl_2$	$SiCl_4/H_2$	50/50	50	0	300	a-Si:H	2.44 (0.11)
$SiCl_2$	$SiCl_4/H_2$	50/50	100	0	300	a-Si:H	2.43 (0.12)

[a]The estimated errors for S values are given in parentheses and are generally the standard deviation of the mean of a minimum of 3 values.
[b]Pressure for mixed gas compositions is given in mTorr for each gas.

In contrast, during a-C:N film deposition, scattering coefficients for CN, NH, and NH_2 appear to have some dependence on gas composition and substrate bias, although each molecule responds differently to these parameter changes [47]. The most dramatic effect is seen with the NH_2 molecules, as $S(NH_2)$ increases significantly from $S = 0.40 \pm 0.10$ to $S = 0.80 \pm 0.10$ as the fraction of NH_3 in the feed gas increases from 30 to 100 %, Table 2. Interestingly, applying a +200 V bias on the substrate leads to a slight reduction in the S values for CN and NH_2. For example, S(CN) measured during the deposition of a-C:N:H films from CH_4/N_2 plasmas is low: $S = 0.15 \pm 0.10$ with no substrate bias, and decreases to $S = 0.02 \pm 0.07$ with +200 V bias, Table 2. S(NH) is essentially constant at various NH_3 fractions, $S = 0.85 \pm 0.07$ under all conditions with $P = 150$ W.

The $S > 1$ values measured for CF_2 and $SiCl_2$ indicate net surface production of these radicals occurs during plasma processing. $S(CF_2)$ values show a clear dependence on applied rf power, increasing from 1.27 ± 0.12 at P = 25 W to 1.65 ± 0.15 at P = 150 W for C_4F_8 plasmas. Placing a g.m. into the path of the molecular beam leads to a decrease in $S(CF_2)$ at all P, and $S(CF_2) \sim 1$ for $P \sim 100$ W. The g.m. acts as a partial physical barrier to plasma species and removes the charged species from the plasma molecular beam [41]. The decrease in scatter measured with the g.m. demonstrates that ions make a significant contribution to the observed CF_2 surface production. Note that although the g.m. removes >85 % of the ionic species from the plasma molecular beam, some ions remain. Thus, $S(CF_2)$ may be <1 under completely ion-free conditions. Experiments in our laboratory are currently underway to explicitly test this hypothesis.

The $S(SiCl_2)$ data show a strong dependence on the gas composition of the $SiCl_4$ plasmas. Specifically, etching of the Si substrate occurs with a 100 % $SiCl_4$ plasma, whereas the 50:50 $SiCl_4/H_2$ plasma leads to deposition of an a-Si:H film. Although surface production of $SiCl_2$ is observed under all conditions studied, it is considerably higher under etching conditions, $S(SiCl_2)$ = 3.5–4.2 for the 100 % $SiCl_4$ systems, than during film deposition, $S(SiCl_2)$ ~2.4 ± 0.1 in the $SiCl_4/H_2$ systems. Moreover, the amount of $SiCl_2$ produced increases dramatically with P, similar to the results for CF_2 in the C_4F_8 system.

Mass spectral data

Figure 6 shows a typical mass spectrum of nascent positive ions present in a 100 W C_4F_8 plasma molecular beam. The C_4F_8 molecules are ionized and dissociated into a variety of fluorocarbon ions in the plasmas, the most intense signals arising from CF_x^+ (x = 1–3), $C_2F_4^+$, $C_3F_3^+$, and $C_3F_5^+$. These data are consistent with our published spectra for this system collected using a different MS with a lower resolution and mass range [40,48]. As discussed elsewhere [41,49], the total ion intensity in the C_4F_8 plasma increases with P up to ~100 W and then levels off at higher P. In addition, the total ion intensity increases as the source pressure increases from 15 to 25 mTorr, and then decreases at higher pressures.

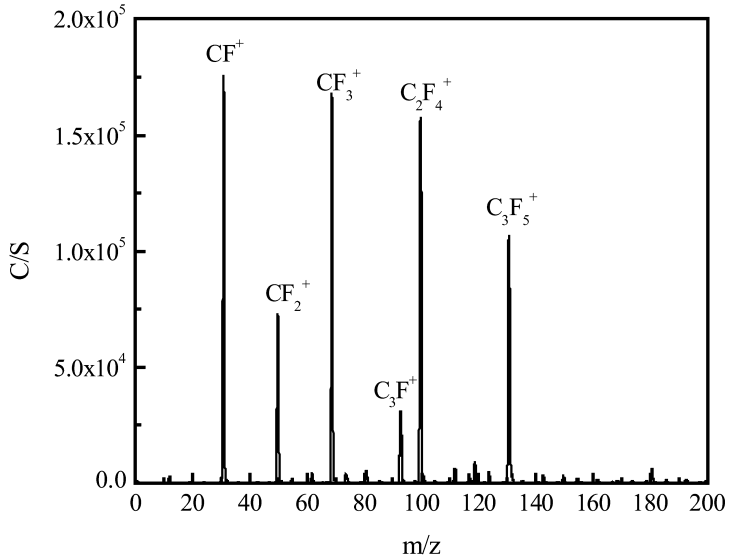

Fig. 6 Typical mass spectra of the positive ion species in a 100 W C_4F_8 plasma. The total pressure in the plasma source was 45 mTorr.

Figure 7 shows the IEDs of the six major ions present in the C_4F_8 plasma. These ions are accelerated in the plasma sheath, and their energies at P = 100 W are typically in the range of 40–90 eV. In general, the ions characterized in many of the different deposition systems (CH_4, CH_4/N_2, CH_4/NH_3, and C_4F_8 plasmas) were found to be energetic, with their mean ion energy increasing with P. As can be seen from the Table 2 data, scatter coefficients measured under ion-limited conditions (using a g.m. or positively biased substrate) were lower than those measured in unperturbed systems. In these cases, the energetic ions contribute to surface production of radicals during plasma-surface interaction. Moreover, in the FC plasma systems, we have found a direct correlation between mean ion energies and $S(CF_2)$ [40,49].

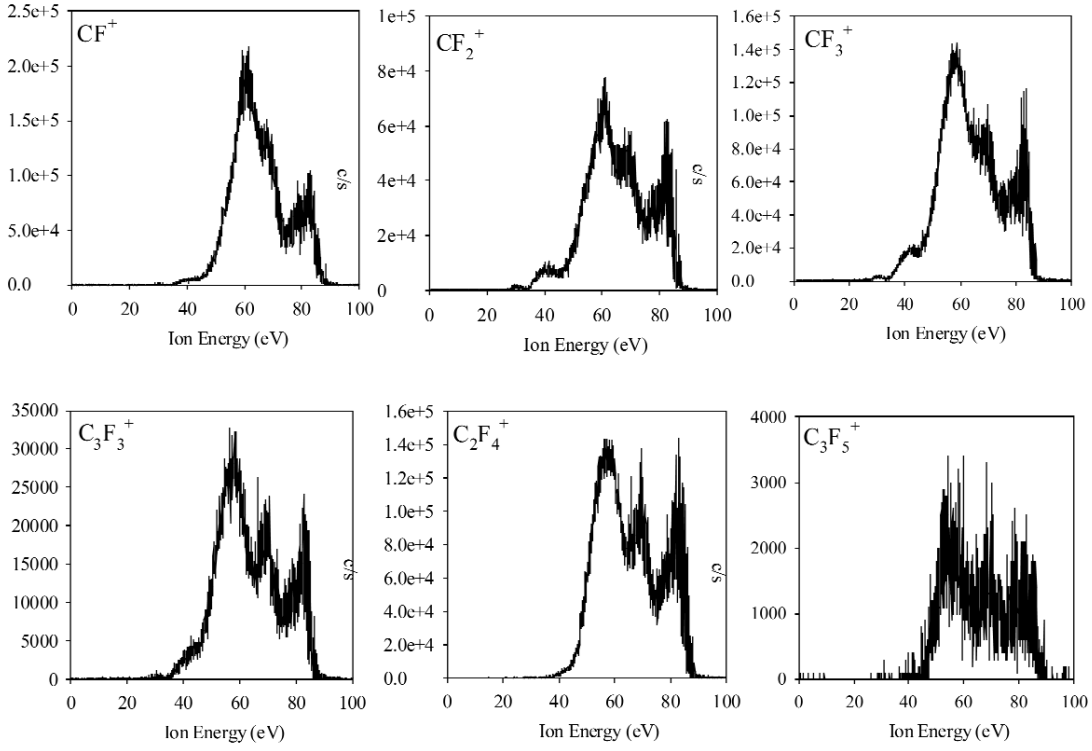

Fig. 7 IEDs of CF^+, CF_2^+, CF_3^+, $C_3F_3^+$, $C_2F_4^+$, and $C_3F_5^+$ in a 100 W C_4F_8 plasma molecular beam. The total pressure in the plasma source was 45 mTorr.

DISCUSSION

Film growth via PECVD is a complicated process involving radical-surface reactions and energetic ion bombardment. For researchers attempting to model the process, some simplifying assumptions must be made. As noted in the Introduction, one of these has been that coordinately unsaturated species react at surfaces with 100 % probability. In other words, radicals are just "sticky". The data presented here (Fig. 5 and Table 2) for molecule-surface interactions during film deposition clearly indicate that this assumption is not valid for all plasma species under all conditions. It is useful, however, to examine these data with respect to the "stickiness" of the molecules we have investigated with IRIS.

The extremely low scattering coefficients of CH and SiH radicals indicate that they are very active at the hydrogenated surface of a-C:H and a-Si:H films, respectively. These radicals could be reacting with surface hydrogen atoms or radical surface sites (dangling bonds) and, thereby contribute to the

film growth. Alternatively, they could be reacting to form other species such as CH_x or SiH_x (x = 2–4), which could then desorb from the surface. Regardless of their loss mechanisms, the similar reactivity observed for CH and SiH radicals may be explained by examining their electronic structures. These isoelectronic molecules are both doublets, with a lone pair of electrons and an unpaired electron on the C or Si atom. The observation that these species are both highly reactive could suggest that the hypothesis regarding radical-surface reactivity is valid. Moreover, it also indicates that a radical's surface reactivity may be an inherent property, which is determined by electronic configuration.

Continuing to examine our IRIS data with respect to reactivity, the low S(CN) values indicate that CN radicals are also very "sticky" during film deposition. One possible gas-surface loss reaction for CN is the H-atom abstraction reaction to form HCN, which could desorb from the surface. Note that CN is also a doublet molecule with an unpaired electron on the carbon atom and a lone pair of electrons on the nitrogen atom. Interestingly, S(CN) ~ 0, identical to S(CH) and S(SiH), upon removal of ion bombardment through substrate biasing. Thus, CN can also be classified as a sticky molecule, which may be related to its doublet electron configuration.

Data for one other doublet species, NH_2, is also given in Table 2. Similar to the other doublet species, NH_2 has both a lone pair of electrons and an unpaired electron on the nitrogen atom. We have previously examined the surface interactions of NH_2 under a variety of conditions, primarily during surface modification of polymers wherein no net film deposition occurs, merely implantation of functional groups [50–52]. In those systems, we found that $S(NH_2) > 1$ under many conditions, but that it decreases upon removal of ions from the molecular beam using the g.m. Here, we have examined the surface interactions of NH_2 under film deposition conditions, and find $S(NH_2)$ shows a clear dependence on the gas composition, yet is always less than unity. NH_2 can react with bonded hydrogen atoms to form NH_3, which can easily desorb from the surface, thereby producing a "dangling bond" site on the growing film surface. Likewise, NH_2 can also be a product of a surface recombination reaction between hydrogen atoms and $–NH_x$ groups at the film surface. Thus, the observed scatter could be a combination of loss at the surface, with compensating formation reactions accounting for the observed desorption of NH_2. Interestingly, however, removal of ions from the plasma-surface interaction does not alter the observed NH_2 scatter under deposition conditions. This suggests that neutralization/desorption reactions as well as physical sputtering are not contributing significantly to the observed scatter. Interestingly, we have measured the N/C ratios of deposited a-C:N:H films by X-ray photoelectron spectrometry (XPS) [53], revealing that nitrogen content at the film surface increases significantly with NH_3 or N_2 fraction in the feed gas. This suggests the $–NH_2$ density at the film surface is higher at high NH_3 or N_2 fractions, which could contribute to the observed increase in $S(NH_2)$ with NH_3 fraction, Table 2. Thus, although NH_2 is a doublet species, it is not as reactive as CH, SiH, and CN radicals. We would categorize its reactivity as moderate.

Although not presented here, we have previously measured surface interactions for two other doublet species, SiF ($A^2\Sigma^+$-$X^2\Pi$) and OH ($A^2\Sigma^+$-$X^2\Pi$), which is isoelectronic with NH_2. These species also exhibit moderate reactivity during film deposition, similar to that seen here for NH_2. Specifically, S(SiF) = 0.3–1 during deposition of a-Si:H from SiF_4/H_2 plasmas [54], S(SiF) = 0.04–0.27 during deposition of SiO_2 from SiF_4/O_2 plasmas [55], and S(OH) ~ 0.6 during deposition of SiO_2 from a variety of alkoxysilane/O_2 (or N_2O) plasmas [56] on unbiased room temperature Si substrates. There are several possible explanations for the observed differences in the reactivity of these doublet species. First, it may be related to the relative electronegativities of the atoms and thus the permament dipole of the molecules. Specifically, the molecules with stronger dipole moments (i.e., SiF, OH, NH_2) appear to be less reactive than those species with smaller dipole moments (i.e., CH, SiH, CN). Second, the reactivities of these gas-phase species may be related to the availability of reaction partners on the surface. If there is a viable reaction partner available on the surface, the molecule can react. For CH, SiH, and CN in the a-C:H, a-SiH, and a-C:N:H deposition systems, there is a sufficient quantity of surface hydrogen to expect that hydrogen abstraction reactions will be favored, even at elevated T_S. We have previously

used this type of argument to explain the T_S dependence of S(OH) during deposition of SiO_2 films. Specifically, OH shows a marked increase in scatter as the T_S increases, most likely because as T_S increases, surface reaction partners such as Si-OH groups are no longer available. A third possibility is that it is difficult to generate CH, SiH, and CN as gas-phase products of plasma-surface interactions. In contrast, there are likely reaction pathways to surface generation of OH, SiF, and NH_2 (reactions 1–3, where * indicates a radical surface site) in the systems of study.

$$O(g) + H(ads) \rightarrow OH(ads) \rightarrow OH(g) + * \quad (1)$$

$$SiF_2 + 2* \rightarrow SiF(ads) + F(ads) \rightarrow SiF(g) + F(s) \quad (2)$$

$$NH(g) + H(ads) \rightarrow NH_2(ads) \rightarrow NH_2(g) + * \quad (3)$$

Regardless of the mechanism at play in these systems, it is clear from these data that doublet species are important to film deposition processes and that further examination of such species via IRIS experiments will continue to help elucidate on the molecular-level chemistry occurring in these complex systems.

To date, we have only examined the surface interactions of one triplet species, NH. The ground state of NH has a lone pair of electrons on the nitrogen atom along with two unpaired electrons. This would suggest that NH should be even more reactive than the doublet species we have examined. In contrast, however, we find that NH scatters with nearly ~100 % probability under a variety of conditions, Table 2. Indeed, in past studies of this molecule we have found that the surface reactivity of NH ranges from ~0.5 to 2.6 under nondepositing conditions (e.g., surface modification systems) [50], and is essentially unity during deposition of silicon nitride films [35]. The nearly unit scattering coefficients measured for NH measured under the film deposition conditions considered here suggests that NH is not active during film formation. This agrees with previous IRIS results for reaction of NH at the surface of a depositing silicon nitride film [35]. Although not strictly analogous, it is interesting to note that the gas-phase reactivity of triplet NH is significantly lower than that of the singlet NH, particularly in reactions involving bond insertion by NH [29,30]. Thus, despite having two unpaired electrons, we find that the triplet NH is not very reactive with the surface of the depositing a-C:N films.

In contrast to all of the other species discussed above, the isoelectronic molecules CF_2 and $SiCl_2$ are both singlet species, meaning they have no unpaired electrons. Both molecules are clearly produced at the surface during film deposition in the FC and $SiCl_4$ systems discussed here. A third singlet species that we have studied using IRIS is SiF_2 (A^1B_1-X^1A_1 transition) [54,55], which is also isoelectronic with CF_2 and $SiCl_2$. Similar to the CF_2 and $SiCl_2$ results, SiF_2 is also generated [$S(SiF_2) > 1$] at the surface of growing a-Si:H,F and SiO_2 films. As noted above, in gas-phase reactions, singlet species tend to be much more reactive than triplet species, and easily insert into various bonds. Our IRIS results would, however, suggest that the carbene and silylene species studied here are less reactive than either the doublet or triplet species we have examined. This may be related to the inherent stability of these particular carbene and silylenes. Specifically, several theoretical studies have demonstrated that the stability of divalent compounds of the group 14 elements are strongly tied to the singlet–triplet gap, which is directly correlated to the substituents on the central atom [57–59]. The singlet state is stabilized by electron-withdrawing substituents and by substituents, such as halogens, that can donate $p\pi$ electrons into the empty p-orbital on the central atom [59]. Consequently, not only does this suggest that the singlet species we have studied with IRIS, CF_2, $SiCl_2$, and SiF_2, might be less reactive at the surface, they are also likely to be extremely stable reaction products. This latter factor suggests that the surface production we observe from these species may be the result of gas-surface reactions that produce the carbene or silylene as a stable product.

For the a-FC PECVD systems, CF_x radicals have been widely proposed as the "real" monomers in plasma polymerization of fluorocarbon films [6]. The observation that $S(CF_2) > 1$ under all conditions studied with IRIS suggests that CF_2 radicals may not be active growth precursors. Interestingly,

however, the surface interactions of CF_2 as well as the other two singlet species behave similarly upon perturbation of the ion population in the plasma molecular beam. Specifically, removal of the ions via the g.m. or substrate biasing leads to a significant decrease in the amount of CF_2 ($SiCl_2$, SiF_2) produced at the surface. This clearly indicates that surface production by ion-induced reactions is occurring. One very real possibility is that CF_2 ($SiCl_2$, SiF_2) generation arises from CF_x^+ ($SiCl_x^+$, SiF_x^+) neutralization (and possibly dissociation) at the growing surface [40].

As a final note on this group of molecules, the $S(SiCl_2) > 2$ values measured in both $SiCl_4$ and $SiCl_4/H_2$ plasmas clearly indicate $SiCl_2$ radicals are the product of plasma-surface interactions in both of these systems. Indeed, the S values measured under etching conditions (100 % $SiCl_4$) are the largest we have ever measured with IRIS, and correlate well with the hypothesis that $SiCl_2$ is a product of chlorine atom etching of Si [60], and is formed via the surface recombination of SiCl and Cl atoms. Although the results shown here are limited in scope, additional experiments are underway to fully characterize the surface interactions of $SiCl_2$ as a function of various parameters. In addition, we plan to examine the surface interactions of SiCl radicals in these systems, which will allow us to explore the effect of the proposed recombination reaction. If $SiCl_2$ formation is the by-product of such a reaction, we anticipate $S(SiCl) < 1$. Moreover, given the doublet configuration of SiCl, this could provide additional evidence in support of one of our hypotheses regarding the surface interactions of nominally sticky molecules (doublets) with a permanent dipole moment.

As noted in the Introduction, one goal of this work is to explore some of the common assumptions made about radical-surface interactions in view of our IRIS results. One of these assumptions is that all radicals have a unit sticking probability under all conditions. This is supported by our IRIS investigations of CH, SiH, and CN radicals in depositing systems—a net surface reactivity of ~0.9–1 was measured under most conditions. In contrast, IRIS reactivity measurements of NH, NH_2, CF_2, and $SiCl_2$ show that these molecules are not nearly as reactive, and in some cases are actually produced at the surface during film deposition. Our IRIS results have revealed that one of the critical surface production mechanisms in the CF_2 (and possibly $SiCl_2$) studies is energetic ion bombardment of the surface. Furthermore, recent work in our group has shown a strong correlation between $S(CF_2)$ and average ion energies in the FC plasmas [41]. Additional work is currently underway to determine if similar correlations can be made between ions and other singlet species generated at the surface of depositing films.

SUMMARY

We have investigated the surface reactivity of various radicals, including CH, SiH, CN, NH_2, NH, CF_2, and $SiCl_2$ during film growth by rf plasmas. These species exhibit a wide range of surface interactions during PECVD processes. Radicals such as CH, SiH, and CN are very sticky, whereas other radicals such as NH, NH_2, CF_2, and $SiCl_2$ are not nearly as reactive during film growth. Isoelectronic pairs such as CH/SiH, NH_2/OH, and $CF_2/SiCl_2/SiF_2$ appear to react very similarly at the surface, suggesting that electronic configuration directs the radical-surface interactions. Ionic species in the plasma also contribute to the observed reactivity. This is especially important for the surface interactions of singlet species such as $SiCl_2$ and CF_2, which can be stable products of plasma-surface reactions. Overall, the data presented here represents over a decade of work using IRIS measurements as a tool to unravel plasma-surface interactions on a molecular level. Clearly, these data demonstrate that attempting to fully understanding radical-surface interactions is indeed a "sticky" situation.

ACKNOWLEDGMENTS

Financial support for this work was provided by the National Science Foundation (NSF-0137664). Additionally, the authors gratefully acknowledge the work of previous coworkers, including Dr. Katherine Bogart, Dr. Carmen Butoi, Dr. Neil Mackie, Dr. Patrick McCurdy, Dr. Michelle Steen, Dr. Keri Williams, and Dr. Jianming Zhang.

REFERENCES

1. J. C. Angus, P. Koidl, S. Domitz. In *Plasma Deposited Thin Films*, J. Mort, F. Jansen (Eds.), p. 89, CRC, Boca Raton, FL (1986).
2. J. Robertson. *Surf. Coat. Technol.* **50**, 185 (1992).
3. H. Cachet, C. Deslouis, M. Chouiki, B. Saidani, N. M. J. Conway, C. Godet. *J. Electrochem. Soc.* **149**, E233 (2002).
4. J. H. Kim, D. H. Ahn, Y. H. Kim, H. K. Baik. *J. Appl. Phys.* **82**, 658 (1997).
5. D. J. Balazs, C. Hollenstein, H. J. Mathieu. *Plasma Process. Polym.* **2**, 14 (2005).
6. R. d'Agostino, F. Cramarossa, F. Fracassi, F. Illuzzi. In *Plasma Deposition, Treatment and Etching of Polymers*, R. d'Agostino (Ed.), pp. 95–162, Academic Press, San Diego (1990).
7. M. Haidopoulous, S. Turgeon, G. Laroche, D. Mantovani. *Plasma Process. Polym.* **2**, 441 (2005).
8. W. Beyer, R. Carius, M. Lejeune, J. Muller, B. Rech, U. Zastrow. *J. Non-Cryst. Solids* **338–340**, 147 (2004).
9. Y. Hamakawa, W. Ma, H. Okamoto. In *Plasma Deposition of Amorphous Silicon-Based Materials*, G. Bruno, P. Cappezzuto, M. Madan (Eds.), pp. 283–314, Academic Press, San Diego (1995).
10. S. Jung, Y. Fujimura, T. Ito, H. Shirai. *Solar Energy Mater. Solar Cells* **74**, 421 (2002).
11. G. Herzberg. *The Spectra and Structures of Simple Free Radicals*, Cornell University, Ithaca, NY (1971).
12. M. W. Kiehlbauch, D. B. Graves. *J. Vac. Sci. Technol., A* **21**, 116 (2003).
13. J. Yun, D. S. Dandy. *Diamond Relat. Mater.* **14**, 1432 (2005).
14. A. von Keudell, M. Meier, T. Schwarz-Selinger. *Appl. Phys. A* **72**, 551 (2001).
15. A. von Keudell, M. Meier, T. Schwarz-Selinger, W. Jacob. *J. Appl. Phys.* **89**, 2979 (2001).
16. A. Kono, N. Koike, H. Nomura, T. Goto. *Jpn. J. Appl. Phys.* **34**, 307 (1995).
17. P. A. Longeway, H. A. Weakliem, R. D. Estes. *J. Phys. Chem.* **88**, 3282 (1984).
18. T. Shirafuji, K. Tachibana, Y. Matsui. *Jpn. J. Appl. Phys.* **34**, 4239 (1995).
19. A. Kono, S. Hirose, K. Kinoshita, T. Goto. *Jpn. J. Appl. Phys.* **37**, 4588 (1998).
20. M. Horie. *J. Vac. Sci. Technol., A* **13**, 2490 (1995).
21. S. J. Limb, C. B. Labelle, K. K. Gleason, D. J. Gleason. *Appl. Phys. Lett.* **68**, 2810 (1996).
22. A. Milella, F. Palumbo, P. Favia, G. Cicala, R. d'Agostino. *Pure Appl. Chem.* **77**, 399 (2005).
23. M. Hertl, J. Jolly. *J. Phys. D: Appl. Phys.* **33**, 381 (2000).
24. J. Perrin, M. Shiratani, P. Kae-Nune, H. Videlot, J. Jolly, J. Guillon. *J. Vac. Sci. Technol., A* **16**, 278 (1998).
25. J. P. Booth. *Plasma Sources Sci. Technol.* **8**, 249 (2000).
26. M. Shiratani, H. Kawasaki, T. Fukuzawa, Y. Watanabe, Y. Yammamoto, M. Suganuma, M. Hori, T. Goto. *J. Phys. D: Appl. Phys.* **31**, 776 (1998).
27. E. R. Fisher. *Plasma Process. Polym.* **1**, 13 (2004).
28. E. R. Fisher. *Plasma Sources Sci. Technol.* **11**, A105 (2002).
29. W. Hack, K. Rathmann. *J. Phys. Chem.* **94**, 3636 (1990).
30. W. Hack, A. Wilms. *J. Phys. Chem.* **93**, 3540 (1989).
31. P. R. McCurdy, K. H. A. Bogart, N. F. Dalleska, E. R. Fisher. *Rev. Sci. Instrum.* **68**, 1684 (1997).
32. K. H. A. Bogart, J. P. Cushing, E. R. Fisher. *J. Phys. Chem. B* **101**, 10016 (1997).
33. K. H. Becker, H. H. Brenig, T. Tatarczyk. *Chem. Phys. Lett.* **71**, 242 (1980).
34. P. W. Fairchild, G. P. Smith, D. R. Crosley, J. B. Jeffries. *Chem. Phys. Lett.* **107**, 181 (1984).
35. E. R. Fisher, P. Ho, W. G. Breiland, R. J. Buss. *J. Phys. Chem.* **96**, 9855 (1992).
36. J. B. Halpern, G. Hancock, M. Lenzi, K. H. Welge. *J. Chem. Phys.* **63**, 4808 (1975).
37. K. A. Mohamed, G. C. King, F. H. Read. *J. Electron Spectrosc. Relat. Phenom.* **12**, 229 (1977).
38. D. S. King, P. K. Schenck, J. C. Stephenson. *J. Mol. Spectrosc.* **78**, 1 (1979).
39. R. C. Sausa, A. M. Ronn. *Chem. Phys.* **96**, 183 (1985).

40. I. T. Martin, E. R. Fisher. *J. Vac. Sci. Technol., A* **22**, 2168 (2004).
41. I. T. Martin, J. Zhou, E. R. Fisher. *J. Vac. Sci. Technol., A* (2006). In press.
42. J. Zhou. Ph.D. thesis, Colorado State University (2006).
43. J. Zhou, R. Ayers, E. Adams, I. T. Martin, D. Liu, E. R. Fisher. *Plasma Sources Sci. Technol.* (2006). Submitted for publication.
44. W. M. M. Kessels, P. R. McCurdy, K. L. Williams, G. R. Barker, V. A. Venturo, E. R. Fisher. *J. Phys. Chem. B* **106**, 2680 (2002).
45. G. Lombardi, K. Hassouni, F. Benedic, F. Mohasseb, J. Ropcke, A. Gicquel. *J. Appl. Phys.* **96**, 6739 (2004).
46. A. V. Filippov, Y. A. Mankelevich, A. F. Pal, T. V. Rakhimova, A. N. Ryabinkin, A. O. Serov, A. Y. Yuriev. 17th International Symposium on Plasma Chemistry, Toronto, Canada, August 7–12 (2005), ID13.
47. D. Liu, I. T. Martin, J. Zhou, E. R. Fisher. (2006). Manuscript in preparation
48. K. L. Williams, I. T. Martin, E. R. Fisher. *J. Am. Soc. Mass. Spectrom.* **13**, 518 (2002).
49. I. T. Martin. Ph.D. thesis, Colorado State University (2005).
50. M. L. Steen, K. R. Kull, E. R. Fisher. *J. Appl. Phys.* **92**, 55 (2002).
51. C. I. Butoi, M. L. Steen, J. R. D. Peers, E. R. Fisher. *J. Phys. Chem. B* **105**, 5957 (2001).
52. P. R. McCurdy, C. I. Butoi, K. L. Williams, E. R. Fisher. *J. Phys. Chem. B* **103**, 6919 (1999).
53. D. Liu, J. Zhou, I. T. Martin, E. R. Fisher. *J. Appl. Phys.* (2006). Manuscript in preparation.
54. K. L. Williams, C. I. Butoi, E. R. Fisher. *J. Vac. Sci. Technol., A* **21**, 1688 (2003).
55. J. Zhang, E. R. Fisher. *J. Appl. Phys.* **96**, 1094 (2004).
56. J. Zhang, E. R. Fisher. *J. Phys. Chem. B* **108**, 9821 (2004).
57. J. Olah, F. De Proft, T. Veszpremi, P. Geerlings. *J. Phys. Chem. A* **109**, 1608 (2005).
58. P. Perez. *J. Phys. Chem. A* **107**, 522 (2003).
59. S. K. Shin, W. A. Goddard III, J. L. Beauchamp. *J. Phys. Chem.* **94**, 6963 (1990).
60. G. P. Kota, D. B. Graves, J. W. Coburn. *J. Vac. Sci. Technol., A* **16**, 270 (1998).
61. F. Seitz, D. Turnbull. *Solid State Phys.* **2**, 305 (1956).
62. W. Bauer, K. H. Becker, R. Duren, C. Hubrich, R. Meuser. *Chem. Phys. Lett.* **108**, 560 (1984).